Study on Current Drive Capability of Lower Hybrid Waves and Neutral Beam in an ITER Steady State Scenario

T. Oikawa 1), M. Shimada 1), A.R. Polevoi 1), O. Naito 2), P.T. Bonoli 3), N. Hayashi 2), C.E. Kessel 4) and T. Ozeki 2)
1) ITER International Team, Naka Joint Work Site, Naka, Ibaraki, Japan
2) Japan Atomic Energy Agency, Naka, Ibaraki, Japan
3) Plasma Science and Fusion Center, MIT, Cambridge, MA, USA
4) Princeton Plasma Physics Laboratory, Princeton, NJ, USA

e-mail contact of main author: oikawa.toshihiro@jaea.go.jp

Abstract. The current drive capability of lower hybrid waves is assessed for an ITER steady state scenario using a relativistic, one-dimensional Fokker-Planck code and a toroidal ray tracing code. The present LH launcher design provides a current drive efficiency of 1.8×10^{19} $\mathrm{AW^{-1}m^{-2}}$ and an off-axis profile of the driven current that is favorable for a reversed magnetic shear configuration. Possible optimizations in the LH power spectrum are investigated. Neutral beam current drive (NBCD) is investigated with theoretical codes employing different approaches. An NBCD code employing the bounce-averaged Fokker-Planck equation to include orbit effects in a toroidal system shows good agreement with an orbit following Monte-Carlo code.

1 Introduction

The initial ITER installation includes 33 MW of neutral beam injection (2 injectors, 16.5 MW per injector) at a beam energy of 1 MeV, 20 MW of electron cyclotron wave (ECW) injection and 20 MW of ion cyclotron wave (ICW) injection [1]. A third NB injector (NBI) and upgrades of RF power are considered as upgrade options. Among the initial set of current drive (CD) actuators, neutral beam current drive (NBCD) is the dominant non-inductive CD source for ITER steady state and hybrid scenarios. In addition, there is the bootstrap current. However, additional CD sources are necessary unless it is expected that a large improvement factor in the energy confinement time, $H_{\mathrm{H98y,2}}$, will occur and will provide a high bootstrap current. In addition to the third NBI, lower hybrid current drive (LHCD) would be an attractive CD tool especially for its high off-axis CD capability. In the interests of integrated modelling of steady state and hybrid scenarios for ITER that has been extensively conducted in recent years [2, 3], assessment of CD capabilities based on the first principle and benchmarking among physics codes are required for a reliable projection of ITER steady state and hybrid operations.

A previous study of the ITER steady state operation employing LHCD presented a fully non-inductive CD scenario with $Q > 5$ at the plasma current $I_{\mathrm{p}} = 9\mathrm{MA}$, assuming an a-priori LH current drive efficiency [4]. In this paper we report the assessment of the LHCD capability in ITER steady state scenarios using a physics code employing ray-tracing and the Fokker-Planck approach, and we discuss possible improvements of LHCD in ITER. Benchmarking of LHCD codes is reported in a collaboration paper at this conference coordinated by the Steady State Operation topical group of the International Tokamak Physics Activity (ITPA) [9].

Neutral beam current drive was experimentally validated for central current drive in JT-60U [5, 6]. An off-axis NBCD case, on the other hand, is reported to be inconsistent with theoretical prediction in ASDEX-Upgrade [7]. In parallel with experimental efforts on this issue [8], it is necessary to check the physics models in the NBCD codes. We report benchmarking between a Fokker-Planck code and a Monte Carlo code.

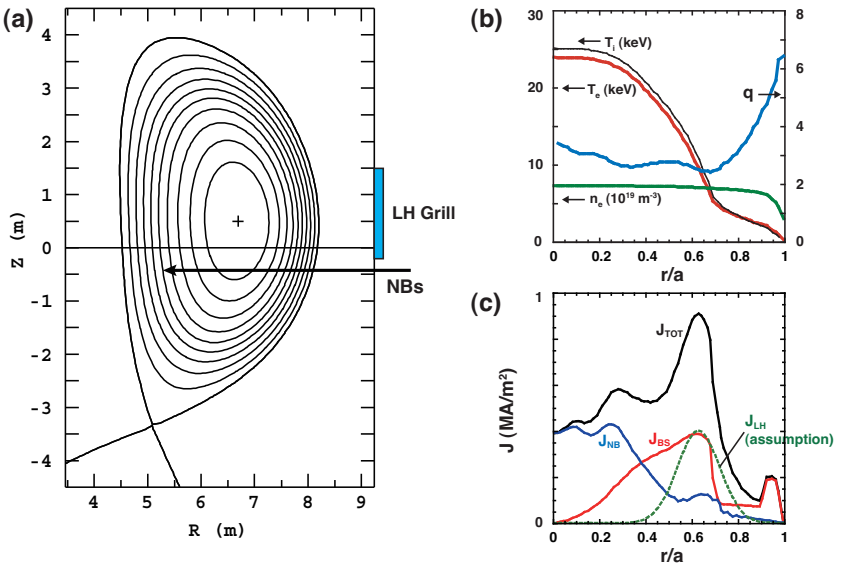

FIG. 1. The reference ITER scenario 4 [4] : **(a)** *Equilibrium and the LH launcher position. Also shown is the poloidal projection of the off-axis NB injection used in the NBCD code benchmark.* **(b)** *The radial profiles of the temperatures, electron density and safety factor, and* **(c)** *the total current density ($J_{\rm TOT}$) and contributions from NBCD ($J_{\rm NB}$), the bootstrap current ($J_{\rm BS}$) and LHCD ($J_{\rm LH}$).*

2 LHCD capability in an ITER steady state scenario

The previous simulation results for the ITER steady state scenario fulfill $Q > 5$ and fully non-inductive CD conditions in a weak reversed magnetic shear configuration by using 33 MW NBI and 37 MW LHW [4]. The equilibrium and plasma profiles are shown in Fig. 1. In this simulation, an a-priori LH current drive efficiency $\eta_{\rm CD} = 3 \times 10^{19}$ AW^{-1}m^{-2} is assumed based on experimental achievements that were conducted with a relatively low parallel index of refraction $n_{\parallel}$ of LHWs. However, in ITER plasmas with the electron density $n_{\rm e} = (7 - 10) \times 10^{19}$m^{-3} and the toroidal magnetic field $B_{\rm T} = 5.3$T at the machine center, low values of $n_{\parallel}$ are limited by the accessibility condition for LHWs. It is necessary to use experimentally validated LHCD codes for reliable prediction of ITER scenarios. We adopt the ACCOME code [10] including as LHCD modules a relativistic, one-dimensional Fokker-Planck code and a toroidal ray tracing code [11], since this code successfully reproduces LHCD profiles measured in JT-60U [12]. The ITER LH launcher consists of four PAM (passive-active multijunction) modules and is designed for installation in an equatorial port [13]. The klystrons operate at 5 GHz. The coupling power per port is 20 MW. Figure 2 (a) shows an injected LH power spectrum against $n_{\parallel}$. The forward lobe of the spectrum (peak at $n_{\parallel} = 2$) contributes to co-directional CD, while the reverse lobe (peak at $n_{\parallel} = -3.3$) drives current in the opposite direction. The directivity of the LH launcher (defined by the fraction of the forward power to the total) is 65-70%. Figure 2 (a) shows calculated profiles of the forward and reverse LH power absorbed by electrons for the reference plasma shown in Fig. 1, where the total LH power is 20 MW corresponding to one launcher and the directivity of the LH spectrum is 70%. As indicated by a rough estimate of the maximum $n_{\parallel}$ for the electron Landau damping, $n_{\parallel}^{\rm abs}({\rm max}) = 6.5/T_{\rm e}^{0.5}$ [14], the forward power is deposited around $r/a = 0.64$ while the reverse power is absorbed in the peripheral region (around $r/a = 0.85$). The LHCD profiles are shown in Fig. 2 (c). The forward and reverse waves drive +0.66 MA and -0.08 MA, respectively. The corresponding current drive efficiency is less than half of the assumption in the previous simulation, while the resultant off-axis LHCD profile is favorable for a steady state scenario with reversed magnetic

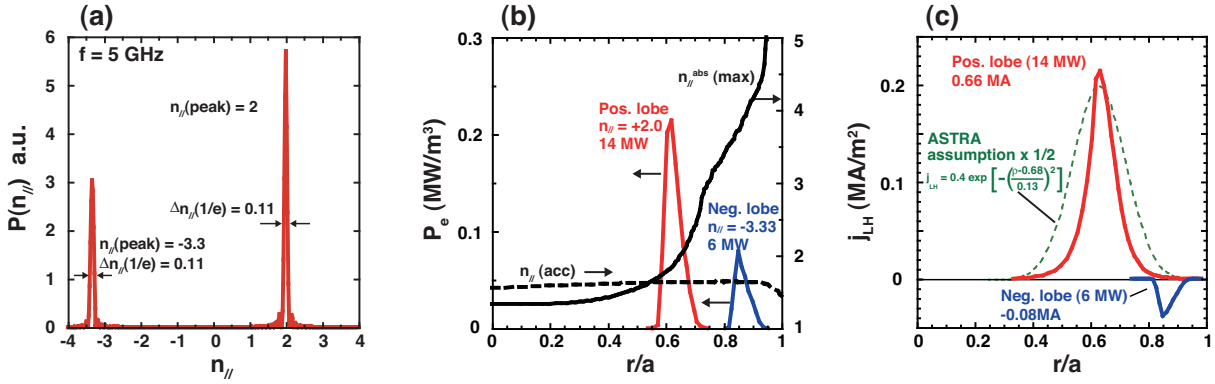

FIG. 2. **(a)** *LH power spectrum vs* $n_{\|}$. **(b)** *Profiles of the absorption power to electrons from the positive and negative lobes of the LH power spectrum (a). Also shown are a rough estimate of the maximum* $n_{\|}$ *for absorption* $n_{\|}^{\rm abs}(\max) = 6.5/T_{\rm e}^{0.5}$ *[14] and the accessibility condition for the plasma.* **(c)** *LHCD profiles for the forward and reverse power, and the assumed profile in the previous simulation (1/2 scale).*

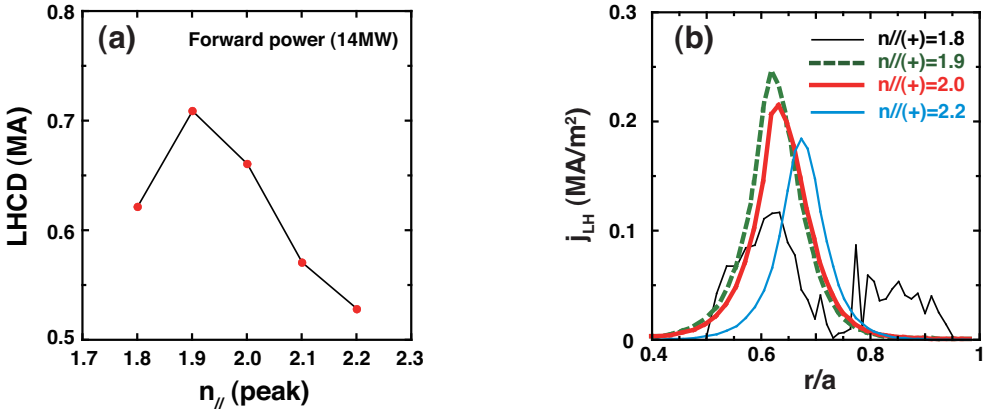

FIG. 3. **(a)** *Peak* $n_{\|}(+)$ *dependence of the LHCD for a forward LH power 14 MW.* **(b)** *LHCD profiles for peak* $n_{\|}(+) = 1.8, 1.9, 2.0$ and 2.2.

shear configuration. This low CD capability results from the low directivity and relatively high $n_{\|}$. Therefore we need to improve LHCD by optimizing the LH power spectrum.

Figure 3 (a) shows a scan of the value of $n_{\|}$ at the positive spectrum peak. LHCD for the forward power scales as $n_{\|}^{-2}$ for $n_{\|} > 1.9$. Decreasing $n_{\|}$ below 1.9, however, deteriorates LHCD. Figure 3 (b) shows LHCD profiles for a $n_{\|}$ scan. With decreasing $n_{\|}$ from 2.2 to 1.9, the absorption region moves inward dependent on the electron temperature. At $n_{\|} = 1.8$, the LHCD profile becomes irregularly broad. This is because the accessibility condition of LHWs, $n_{\|}(\mathrm{acc}) \sim 1 + \omega_{\rm pe}/\omega_{\rm ce}$, is approached as shown in Fig. 2 (b) ($\omega_{\rm pe}$: electron plasma frequency, $\omega_{\rm ce}$: electron cyclotron frequency). Near the accessibility limit, LHWs are less absorbed and $n_{\|}$ suffers up-shift at reflections on the plasma surface during multi-pass absorption. Under these conditions, some fraction of the injected LH power is deposited in the peripheral region. In such a case of multi-pass absorption, the calculated result would be less reliable since the physical mechanisms of $n_{\|}$ upshift during the wave propagation are presently not well understood.

There would be room for optimizing the phase shift (ϕ) between adjacent waveguides of the LH launcher. The directivity of the spectrum can be improved by reducing ϕ since its directivity

is roughly approximated as $(1 - \phi/2\pi)$. However, ϕ has to be $60°$, $90°$ and their harmonics in order to cancel reflected waves and avoid production of electric field at the front of the LH grill. Since the peak $n_{\parallel}$ is $c\phi/\Delta\omega$ (c : light speed, Δ : pitch of adjacent waveguides and ω : frequency of LHWs), Δ or ω need to be reduced for lowering ϕ. There is an engineering limit in Δ coming from heat removal, and with reduced ω, LHWs suffers from absorption by α particles. On the other hand, Ref. [9] reports a favorable result from 2D Fokker-Planck codes showing a 40 % higher current drive than 1D codes including the code employed in this paper.

3 NBCD benchmarking between a Fokker-Planck code and an Orbit Following Monte-Carlo code

We have examined the Fokker-Planck code ACCOME [10] and the Monte Carlo code OFMC [15] for the reference ITER scenario 4 plasma. Both codes have been validated with NBCD experiments in JT-60U [5, 6]. We describe treatments in ACCOME and OFMC of each physics process of NBCD and compare their results.

Birth source of the fast ions:
For the calculation of the source of fast ions, both the ACCOME and OFMC codes adopt the same module based on the Monte-Carlo method. They divide an elliptic cross-section of an NB with a Gaussian intensity profile into a mesh and start beam trace from a mesh point chosen with the Monte-Carlo method. Along with the beam trace, ionization of the fast neutrals are evaluated in the Monte-Carlo manner with Janev's stopping cross-section incorporating the multi-step ionization process [16]. For off-axis NB injection in the scenario 4 plasma (Fig. 1), profiles of the fast ion birth source calculated with ACCOME and OFMC are shown in Fig. 4 (a). The number of the Monte-Carlo particles are 2000 in both calculations. There is a minute difference between the profiles because ACCOME and OFMC adopt different functions for the random number generation on different computers. The difference would become smaller with increasing number of test particles.

Fast ion distribution functiton:
The OFMC code employs an orbit following Monte-Carlo technique and hence necessarily includes the orbit effects in a toroidal system, such as displacement of a particle orbit from a

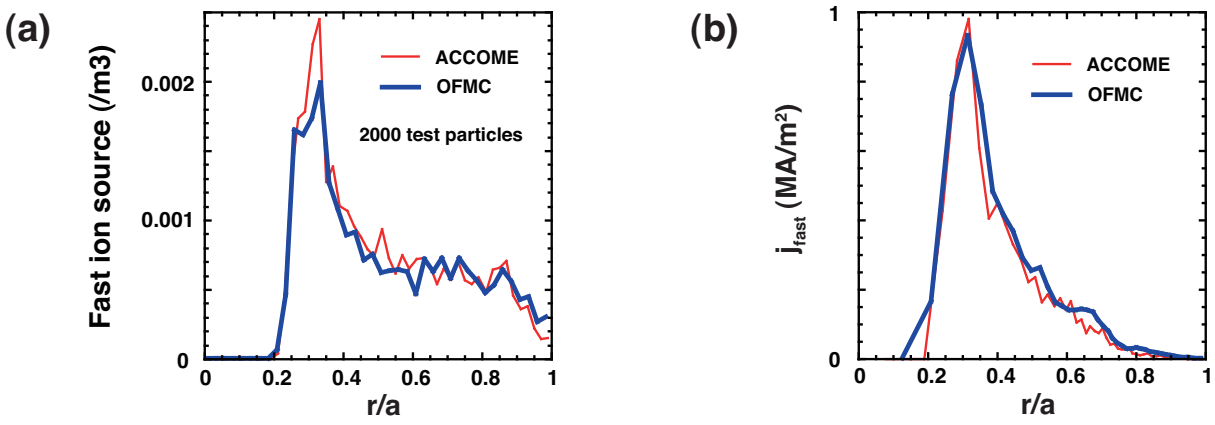

FIG. 4. **(a)** *The reference scenario 4 equilibrium and poloidal projection of the off-axis NB injection. Profiles of* **(b)** *the fast ion source and* **(c)** *the fast ion current density (toroidal) calculated with ACCOME and OFMC.*

magnetic surface, particle trapping and variation of the pitch angle in a bounce motion along a magnetic field line. Also considered is the radial motion of a test particle due to collisions with background thermal species (electrons, fuel ions, He ions and impurities). ACCOME adopts numerically derived eigenfunctions of the bounce-averaged, two-dimensional Fokker-Planck equation [17], while some of other Fokker-Planck codes employ analytical solutions of the non-bounce averaged Fokker-Planck equation that are derived in [18]. Fast ion source profiles are also bounce-averaged in ACCOME. ACCOME also incorporates the energy diffusion term [18] derived in a regime of particle energy larger than an initial injection energy. Once a fast ion distribution function in the velocity space $f(v,\xi)$ (v velocity and ξ pitch angle) is obtained at a spatial point, a local fast ion current density along a magnetic field line is calculated by integrating $\xi v f(v,\xi)$ in the velocity space.

Figure 4 (b) shows a comparison of the fast ion current density profile $j_{\rm fast}$ between ACCOME and OFMC. The profiles agree very well. The OFMC profile is slightly wider than the ACCOME one. This is because radial diffusion of the test particles during slowing down is included in the OFMC calculations. In the Fokker-Planck approach of ACCOME, on the other hand, fast ions stay on the magnetic surfaces where they are initially produced until they become thermalized. The non-circular cross-section of plasmas would be another possible reason for discrepancy, since the bounce averaged Fokker Planck equation adopted in ACCOME is derived for a circular plasma cross-section. Total fast ion currents given by ACCOME and OFMC are 2.7MA and 3.0MA, respectively.

ACCOME does not consider fast ion losses due to the ripple effect and charge exchange (CX) process. Thus, calculations of their effects were turned off in the above OFMC run. The ripple and CX losses are estimated to be 1% and 0.5%, respectively, by OFMC. The shine-through loss is estimated to be negligible in both ACCOME and OFMC.

Electron shielding effect:

The fast ion current determined through the above steps is partially canceled by thermal electrons being dragged along with the fast ions. The net beam driven current $j_{\rm BD}$ can be written in a form,

$$j_{\rm BD} = \mathit{\Gamma}\, j_{\rm fast}, \tag{1}$$

$$\mathit{\Gamma} = 1 - F\left(Z_{\rm b}, Z_{\rm eff}, v/v_{\rm e}^{\rm th}\right)\left(1 - G\left(Z_{\rm eff}, \epsilon\right)\right), \tag{2}$$

where $Z_{\rm b}$ the charge of fast ions, $Z_{\rm eff}$ the effective charge of the plasma ions, v the fast ion velocity, $v_{\rm e}^{\rm th}$ the electron thermal velocity and ϵ the inverse aspect ratio. F represents the fraction of electrons dragged along with the fast ions. This term is generally taken as $Z_{\rm b}/Z_{\rm eff}$, which is originally derived on the assumption that the electrons can be represented by a displaced Maxwellian, corresponding to the condition $v_{\rm e}^{\rm th} \gg v$. This analysis has two shortcomings. First, the velocity dependence of the frictional force between the fast ions and the electrons is generally different from that between the thermal ions and the electrons, which leads to the distorted electron distribution. The second is that electron-electron collisions are not taken into account properly. ACCOME and OFMC adopt a result of the electron Fokker-Planck equation including these effects by Cordey et al [19]. The trapped electron correction term G adopts the work of Start and Cordey [20], who provided a numerical table of G for plasmas in the banana regime with $Z_{\rm eff} = 1 - 16$ and $\epsilon = 0.0 - 0.9$. Figure 5 (a)-(c) show F, G and the total electron shielding factor $\mathit{\Gamma}$, respectively. It is clearly shown that the distortion in the electron distribution function is important in F when the fast ion velocity cannot be ignored compared

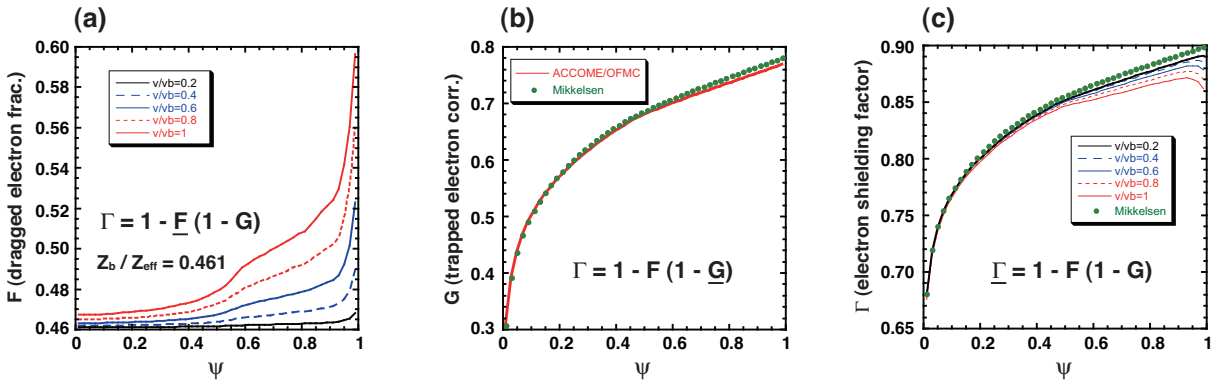

FIG. 5. Electron shielding effect against fast ion flow. **(a)** *Profiles of the electron response term* $F(\psi, v/v_{\rm e}^{\rm th})$ *for* $v/v_{\rm b} = 0.2, 0.4, 0.6, 0.8{\rm and}1.0$*, where* $v/v_{\rm e}^{\rm th}$ *the ratio of the fast ion velocity to the electron thermal velocity and* $v/v_{\rm b}$ *the ratio of the fast ion velocity to the initial beam injection velocity.* **(b)** *Profiles of the trapped electron correction term* $G(\psi)$ *for the implementation in ACCOME/OFMC and Mikkelsen&Singer's fit.* **(c)** *Profiles of the electron shielding factor for ACCOME/OFMC and the Mikkelsen-Singer approximation.*

to the local electron thermal velocity. In the peripheral region ($r/a > 0/7$) of the ITER steady state plasma, the fraction of the electrons dragged by the fast ions is evaluated to be > 10 % higher at the incident beam energy of 1 MeV than $Z_{\rm b}/Z_{\rm eff} = 0.461$. Figure 5 (b) shows G used in ACCOME/OFMC (described by the Start&Cordey model) along with the Mikkelsen and Singer 's fit to the Start&Cordey model [21]. The discrepancy is $\sim 1\%$ even at the edge whose ϵ is outside the range of the fit formula. The total electron shielding factor (Fig. 5 (c)) is by $3-5\%$ different in $r/a > 0.7$ between the $v/v_{\rm b} = 1.0$ case of ACCOME/OFMCC and the Mikkelsen&Singer's fit (which takes $F = Z_{\rm b}/Z_{\rm eff}$). Since the trapped electron correction G becomes large in the peripheral region, the total electron shielding does not differ from the Mikkelsen&Singer's fit as much as F. However, before high electron temperature is reached in a pulse, the finite velocity of the fast ions would be important in all plasma regions including the core, and hence it affects the prediction of evolving plasmas through the NBCD profile.

4 Conclusions

The current drive capability of the lower hybrid waves has been assessed for the reference ITER steady state scenario. We predict that the present LH launcher design will provide 1.2 MA of LHCD for the maximum injection power of 40 MW corresponding to a current drive efficiency of 1.8×10^{19} AW^{-1}m^{-2}. The LH driven current profile would be located around $r/a = 0.64$, which would help create the reversed magnetic shear configuration necessary for good confinement. An optimum spectrum for the reference plasma is obtained at $n_{\|} = 1.9$, giving 10% improvement in LHCD. Neutral beam current drive (NBCD) is investigated with a Fokker-Planck equation based code and an orbit following Monte-Carlo code. The Fokker-Planck code takes into consideration energy diffusion towards the energy regime higher than the incident beam energy and employs the bounce-averaged Fokker-Planck equation in order to include orbit effects. It shows a good agreement with the Monte-Carlo code. For the electron shielding effect, both codes employ trapped electron correction for arbitrary ϵ and the dragged electron fraction for an electron distribution function distorted from Maxwellian by injected fast ions. The latter effect becomes important when the fast ion velocity is not negligible compared to the local electron thermal velocity. In the peripheral region ($r/a > 0/7$) of ITER plasmas,

the fraction of electrons dragged by fast ions is > 10 % higher at the incident beam energy of 1 MeV than a widely used expression of $Z_{\rm b}/Z_{\rm eff}$ that was originally derived for a displaced Maxwellian distribution of electrons.

Acknowledgment

One of the authors (T.O.) would like to thank Masanobu Suzuki, I. Kamata and Mitsuhiro Suzuki for supports in code developments and computing environment, and H. Fujieda and Y. Gribov for provision of equilibrium data and relevant discussions. T.O. also would like to thank V. Mukhovatov for advises and discussions in a wide area of physics.

This report was prepared as an account of work undertaken within the framework of ITER Transitional Arrangements (ITA). These are conducted by the Participants: the European Atomic Energy Community, India, Japan, the People's Republic of China, the Republic of Korea, the Russian Federation, and the United States of America, under the auspices of the International Atomic Energy Agency. The views and opinions expressed herein do not necessarily reflect those of the Participants to the ITA, the IAEA or any agency thereof. Dissemination of the information in this paper is governed by the applicable terms of the former ITER EDA Agreement.

References

[1] SHIMOMURA, Y., et al., PPCF 43 (2001) A385.

[2] HOULBERG, W.A., et al., Nucl. Fusion 45 (2005) 1309.

[3] KESSEL, C.E., et al., this conference, IT/P1-7.

[4] POLEVOI, A.R., et al., Proc. 19th IAEA Fusion Energy Conf. (2002) IAEA-CN-94/CT/P-08.

[5] OIKAWA, T., et al., Nucl. Fusion 40 (2000) 435.

[6] OIKAWA, T., et al., Nucl. Fusion 41 (2001) 1575.

[7] HOBIRK, J., OIKAWA, T., et al., 30th EPS Conf. (2003) O-4.1B.

[8] SUZUKI, T., IDE, S., FUJITA, T., OIKAWA, T., et al., this conference, EX/6-4.

[9] BONOLI, P.T., et al., this conference, IT/P1-2.

[10] TANI, K., AZUMI, M., DEVOTE, R. S., Journal of Computational Physics 98 (1992)332.

[11] BONOLI, P.T. and ENGLADE, R.C., Phys. Fluids 29 (1986) 2937.

[12] NAITO, O., CUI, Z., IDE, S., SUZUKI, T., OIKAWA, T., et al., Phys. Rev. Lett. 89 (2002) 065001-1.

[13] ITER Design Description Document (DDD) 5.4.

[14] BARBATO, E., PPCF 40 (1998) A63.

[15] TANI, K., et al., Journal of Phys. Soc. Jpn. 50 (1981)1726.

[16] JANEV, R.K., BOLEY, C.D. and POST, D.E., Nucl. Fusion 29 (1989) 2125.

[17] CORDEY, J.G., Nucl. Fusion 16 (1976) 499.

[18] Gaffey, J.D., J. Plasma Phys. 16 (1975) 149.

[19] CORDEY, J.G., JONES, E.M. and START, D.F.H., Nucl. Fusion 19 (1979) 249.

[20] START, D.F.H. and CORDEY, J.G., Phys. Flulids 23 (1980) 1477.

[21] MIKKELSEN, D.R. and SINGER, C.E., Nucl. Technol. Fusion 4 (1983) 237.